



BELLE2-CONF-2022-018

November 9, 2022

Measurement of the photon energy spectrum of inclusive hadronic tagged $B \rightarrow X_s \gamma$ decays at Belle II: Approved plots

(The Belle II Collaboration)

F. Abudinén, I. Adachi, K. Adamczyk, L. Aggarwal, P. Ahlburg, H. Ahmed, J. K. Ahn, H. Aihara, N. Akopov, A. Aloisio, F. Ameli, L. Andricek, N. Anh Ky, D. M. Asner, H. Atmacan, V. Aulchenko, T. Aushev, V. Aushev, T. Aziz, V. Babu, S. Bacher, H. Bae, S. Baehr, S. Bahinipati, A. M. Bakich, P. Bambade, Sw. Banerjee, S. Bansal, M. Barrett, G. Batignani, J. Baudot, M. Bauer, A. Baur, A. Beaubien, A. Beaulieu, J. Becker, P. K. Behera, J. V. Bennett, E. Bernieri, F. U. Bernlochner, V. Bertacchi, M. Bertemes, E. Bertholet, M. Bessner, S. Bettarini, V. Bhardwaj, B. Bhuyan, F. Bianchi, T. Bilka, S. Bilokin, D. Biswas, A. Bobrov, D. Bodrov, A. Bolz, A. Bondar, G. Bonvicini, A. Bozek, M. Bračko, P. Branchini, N. Braun, R. A. Briere, T. E. Browder, D. N. Brown, A. Budano, L. Burmistrov, S. Bussino, M. Campajola, L. Cao, G. Casarosa, C. Cecchi, D. Červenkov, M.-C. Chang, P. Chang, R. Cheaib, P. Cheema, V. Chekelian, C. Chen, Y. Q. Chen, Y. Q. Chen, Y.-T. Chen, B. G. Cheon, K. Chilikin, K. Chirapatpimol, H.-E. Cho, K. Cho, S.-J. Cho, S.-K. Choi, S. Choudhury, D. Cinabro, L. Corona, L. M. Cremaldi, S. Cunliffe, T. Czank, S. Das, N. Dash, F. Dattola, E. De La Cruz-Burelo, S. A. De La Motte, G. de Marino, G. De Nardo, M. De Nuccio, G. De Pietro, R. de Sangro, B. Deschamps, M. Destefanis, S. Dey, A. De Yta-Hernandez, R. Dhamija, A. Di Canto, F. Di Capua, S. Di Carlo, J. Dingfelder, Z. Doležal, I. Domínguez Jiménez, T. V. Dong, M. Dorigo, K. Dort, D. Dossett, S. Dreyer, S. Dubey, S. Duell, G. Dujany, P. Ecker, S. Eidelman, M. Eliachevitch, D. Epifanov, P. Feichtinger, T. Ferber, D. Ferlewicz, T. Fillinger, C. Finck, G. Finocchiaro, P. Fischer, K. Flood, A. Fodor, F. Forti, A. Frey, M. Friedl, B. G. Fulsom, M. Gabriel, A. Gabrielli, N. Gabyshev, E. Ganiev, M. Garcia-Hernandez, R. Garg, A. Garmash, V. Gaur, A. Gaz, U. Gebauer, A. Gellrich, J. Gemmler, T. Geßler, G. Ghevondyan, G. Giakoustidis, R. Giordano, A. Giri, A. Glazov, B. Gobbo, R. Godang, P. Goldenzweig, B. Golob, P. Gomis, G. Gong, P. Grace, W. Gradl, S. Granderath, E. Graziani, D. Greenwald, T. Gu, Y. Guan, K. Gudkova, J. Guilliams, C. Hadjivasilou, S. Halder, K. Hara, T. Hara, O. Hartbrich, K. Hayasaka, H. Hayashii, S. Hazra, C. Hearty, M. T. Hedges, I. Heredia de la Cruz, M. Hernández Villanueva, A. Hershenhorn, T. Higuchi, E. C. Hill, H. Hirata, M. Hoek, M. Hohmann, S. Hollitt, T. Hotta, C.-L. Hsu, K. Huang, T. Humair, T. Iijima, K. Inami, G. Inguglia, N. Ipsita, J. Irakkathil Jabbar, A. Ishikawa, S. Ito, R. Itoh, M. Iwasaki, Y. Iwasaki, S. Iwata, P. Jackson, W. W. Jacobs, D. E. Jaffe, E.-J. Jang, M. Jeandron, H. B. Jeon, Q. P. Ji, S. Jia, Y. Jin, C. Joo, K. K. Joo, H. Junkerkalefeld, I. Kadenko, J. Kahn, H. Kakuno, M. Kaleta, A. B. Kaliyar, J. Kandra, K. H. Kang, S. Kang, P. Kapusta, R. Karl, G. Karyan, Y. Kato, H. Kawai, T. Kawasaki, C. Ketter, H. Kichimi, C. Kiesling, C.-H. Kim, D. Y. Kim, H. J. Kim, K.-H. Kim, K. Kim,

S.-H. Kim, Y.-K. Kim, Y. Kim, T. D. Kimmel, H. Kindo, K. Kinoshita, C. Kleinwort, B. Knysh, P. Kodyš, T. Koga, S. Kohani, K. Kojima, I. Komarov, T. Konno, A. Korobov, S. Korpar, N. Kovalchuk, E. Kovalenko, R. Kowalewski, T. M. G. Kraetzschmar, F. Krinner, P. Križan, R. Kroeger, J. F. Krohn, P. Krokovny, H. Krüger, W. Kuehn, T. Kuhr, J. Kumar, M. Kumar, R. Kumar, K. Kumara, T. Kumita, T. Kunigo, M. Künzel, S. Kurz, A. Kuzmin, P. Kvasnička, Y.-J. Kwon, S. Lacaprara, Y.-T. Lai, C. La Licata, K. Lalwani, T. Lam, L. Lanceri, J. S. Lange, M. Laurenza, K. Lautenbach, P. J. Laycock, R. Leboucher, F. R. Le Diberder, I.-S. Lee, S. C. Lee, P. Leitl, D. Levit, P. M. Lewis, C. Li, L. K. Li, S. X. Li, Y. B. Li, J. Libby, K. Lieret, J. Lin, Z. Liptak, Q. Y. Liu, Z. A. Liu, D. Liventsev, S. Longo, A. Loos, A. Lozar, P. Lu, T. Lueck, F. Luetticke, T. Luo, C. Lyu, C. MacQueen, M. Maggiora, R. Maiti, S. Maity, R. Manfredi, E. Manoni, A. Manthei, S. Marcello, C. Marinas, L. Martel, A. Martini, L. Massaccesi, M. Masuda, T. Matsuda, K. Matsuoka, D. Matvienko, J. A. McKenna, J. McNeil, F. Meggendorfer, F. Meier, M. Merola, F. Metzner, M. Milesi, C. Miller, K. Miyabayashi, H. Miyake, H. Miyata, R. Mizuk, K. Azmi, G. B. Mohanty, N. Molina-Gonzalez, S. Moneta, H. Moon, T. Moon, J. A. Mora Grimaldo, T. Morii, H.-G. Moser, M. Mrvar, F. J. Müller, Th. Muller, G. Muroyama, C. Murphy, R. Mussa, I. Nakamura, K. R. Nakamura, E. Nakano, M. Nakao, H. Nakayama, H. Nakazawa, A. Narimani Charan, M. Naruki, Z. Natkaniec, A. Natochii, L. Nayak, M. Nayak, G. Nazaryan, D. Neverov, C. Niebuhr, M. Niijima, J. Ninkovic, N. K. Nisar, S. Nishida, K. Nishimura, M. H. A. Nouxman, K. Ogawa, S. Ogawa, S. L. Olsen, Y. Onishchuk, H. Ono, Y. Onuki, P. Oskin, F. Otani, E. R. Oxford, H. Ozaki, P. Pakhlov, G. Pakhlova, A. Paladino, T. Pang, A. Panta, E. Paoloni, S. Pardi, K. Parham, H. Park, S.-H. Park, B. Paschen, A. Passeri, A. Pathak, S. Patra, S. Paul, T. K. Pedlar, I. Peruzzi, R. Peschke, R. Pestotnik, F. Pham, M. Piccolo, L. E. Piilonen, G. Pinna Angioni, P. L. M. Podesta-Lerma, T. Podobnik, S. Pokharel, L. Polat, V. Popov, C. Praz, S. Prell, E. Prencipe, M. T. Prim, M. V. Purohit, H. Purwar, N. Rad, P. Rados, S. Raiz, A. Ramirez Morales, R. Rasheed, N. Rauls, M. Reif, S. Reiter, M. Remnev, I. Ripp-Baudot, M. Ritter, M. Ritzert, G. Rizzo, L. B. Rizzuto, S. H. Robertson, D. Rodríguez Pérez, J. M. Roney, C. Rosenfeld, A. Rostomyan, N. Rout, M. Rozanska, G. Russo, D. Sahoo, Y. Sakai, D. A. Sanders, S. Sandilya, A. Sangal, L. Santelj, P. Sartori, Y. Sato, V. Savinov, B. Scavino, M. Schnepf, M. Schram, H. Schreeck, J. Schueler, C. Schwanda, A. J. Schwartz, B. Schwenker, M. Schwickardi, Y. Seino, A. Selce, K. Senyo, I. S. Seong, J. Serrano, M. E. Sevier, C. Sfienti, V. Shebalin, C. P. Shen, H. Shibuya, T. Shillington, T. Shimasaki, J.-G. Shiu, B. Shwartz, A. Sibidanov, F. Simon, J. B. Singh, S. Skambraks, J. Skorupa, K. Smith, R. J. Sobie, A. Soffer, A. Sokolov, Y. Soloviev, E. Solovieva, S. Spataro, B. Spruck, M. Starić, S. Stefkova, Z. S. Stottler, R. Stroili, J. Strube, J. Stypula, Y. Sue, R. Sugiura, M. Sumihama, K. Sumisawa, T. Sumiyoshi, W. Sutcliffe, S. Y. Suzuki, H. Svidras, M. Tabata, M. Takahashi, M. Takizawa, U. Tamponi, S. Tanaka, K. Tanida, H. Tanigawa, N. Taniguchi, Y. Tao, P. Taras, F. Tenchini, R. Tiwary, D. Tonelli, E. Torassa, N. Toutounji, K. Trabelsi, I. Tsaklidis, T. Tsuboyama, N. Tsuzuki, M. Uchida, I. Ueda, S. Uehara, Y. Uematsu, T. Ueno, T. Uglov, K. Unger, Y. Unno, K. Uno, S. Uno, P. Urquijo, Y. Ushiroda, Y. V. Usov, S. E. Vahsen, R. van Tonder, G. S. Varner, K. E. Varvell, A. Vinokurova, L. Vitale, V. Vobbilisetti, V. Vorobyev, A. Vossen, B. Wach, E. Waheed, H. M. Wakeling, K. Wan, W. Wan Abdullah, B. Wang, C. H. Wang,

E. Wang, M.-Z. Wang, X. L. Wang, A. Warburton, M. Watanabe, S. Watanuki, J. Webb, S. Wehle, M. Welsch, C. Wessel, J. Wiechczynski, P. Wieduwilt, H. Windel, E. Won, L. J. Wu, X. P. Xu, B. D. Yabsley, S. Yamada, W. Yan, S. B. Yang, H. Ye, J. Yelton, J. H. Yin, M. Yonenaga, Y. M. Yook, K. Yoshihara, T. Yoshinobu, C. Z. Yuan, Y. Yusa, L. Zani, Y. Zhai, J. Z. Zhang, Y. Zhang, Y. Zhang, Z. Zhang, V. Zhilich, J. Zhou, Q. D. Zhou, X. Y. Zhou, V. I. Zhukova, V. Zhulanov, and R. Žlebčík

Abstract

We measure the photon energy spectrum of inclusive radiative $B \rightarrow X_s \gamma$ decays in a sample corresponding to 189.3 fb^{-1} of integrated luminosity collected at the $\Upsilon(4S)$ resonance by the Belle II experiment at the SuperKEKB asymmetric-energy e^+e^- collider. The tag-side B candidates are fully reconstructed using a large number of hadronic channels. The partial branching fractions are measured as a function of photon energy in the decaying B meson rest frame, E_γ^B , in eight bins above 1.8 GeV. The integrated partial branching fractions for three thresholds of $E_\gamma^B > 1.8 \text{ GeV}$, 2.0 GeV and 2.1 GeV agree with the world averages.

1 Approved plots

This section contains additional approved plots that are not included in the main conference note. They can be used for conferences and presentation of the analysis.

1.1 Off-resonance data

Continuum suppression classifier training plots are given in Figure 1.

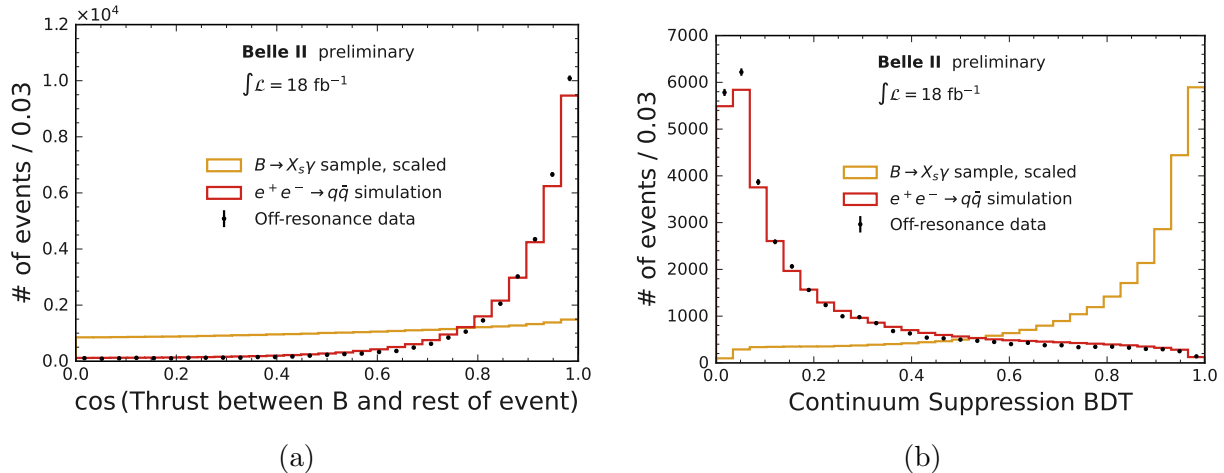


FIG. 1: Plots related to $e^+e^- \rightarrow q\bar{q}$ background event suppression. Various event-topology, B tag kinematics, and vertexing variables are combined in a Boosted Decision Tree (BDT) classifier to reject non- $B\bar{B}$ contribution in data. The most distinguishing variable in the BDT classifier is shown in Figure 1a. The BDT classifier output is shown in Figure 1b. They describe the $e^+e^- \rightarrow q\bar{q}$ distribution well and show good separation of $B \rightarrow X_s \gamma$ events and $e^+e^- \rightarrow q\bar{q}$ events.

After all analysis selections, including continuum-suppression, π^0 and η vetoes, mis-identified photon removal, the $e^+e^- \rightarrow q\bar{q}$ background photon candidate spectrum looks as shown in Figure 2.

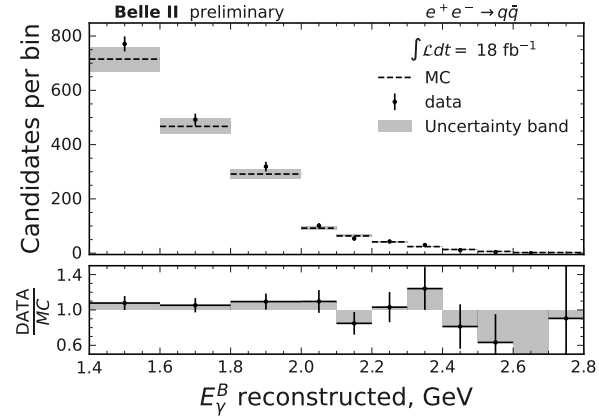


FIG. 2: The $e^+e^- \rightarrow q\bar{q}$ background photon candidate spectrum, after reconstruction and continuum-suppression, π^0 and η vetoes, mis-identified photon removal. Simulated backgrounds show good agreement with data expectations.

1.2 On-resonance data with π^0 ad η rejection requirements inverted

By inverting the π^0 and η rejection requirements we arrive at a sample with an enriched contribution of photon candidates originating in various processes that lead to $\pi^0 \rightarrow \gamma\gamma$ and $\eta \rightarrow \gamma\gamma$, which are background to the signal photon candidates to $B \rightarrow X_s\gamma$. By retaining the other standard selections we suppress the $q\bar{q}$ -decay related background photon contribution and misidentified photon contribution. Therefore, this selection allows to compare background photon distribution originating from $B\bar{B}$ decays between simulated samples and data. This is shown in Figure 3.

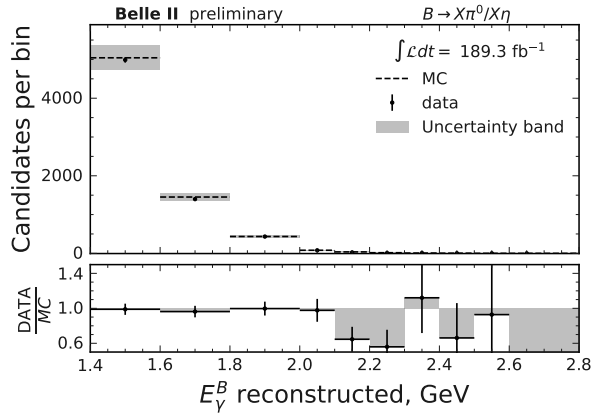


FIG. 3: The $e^+e^- \rightarrow B\bar{B}$ background photon candidate spectrum, after reconstruction and continuum-suppression, mis-identified photon removal. The regular π^0 and η veto rejection requirements are inverted, such that a background enriched sample is obtained. Simulated backgrounds show good agreement with data expectations.

1.3 Continuum suppression and π^0 veto plots in the E_γ^B sideband

Continuum suppression and π^0 veto agreement between simulated samples and data in the photon-energy sideband region ($E_\gamma^B \in [1.4, 1.8]$ GeV) is shown in Figure 4.

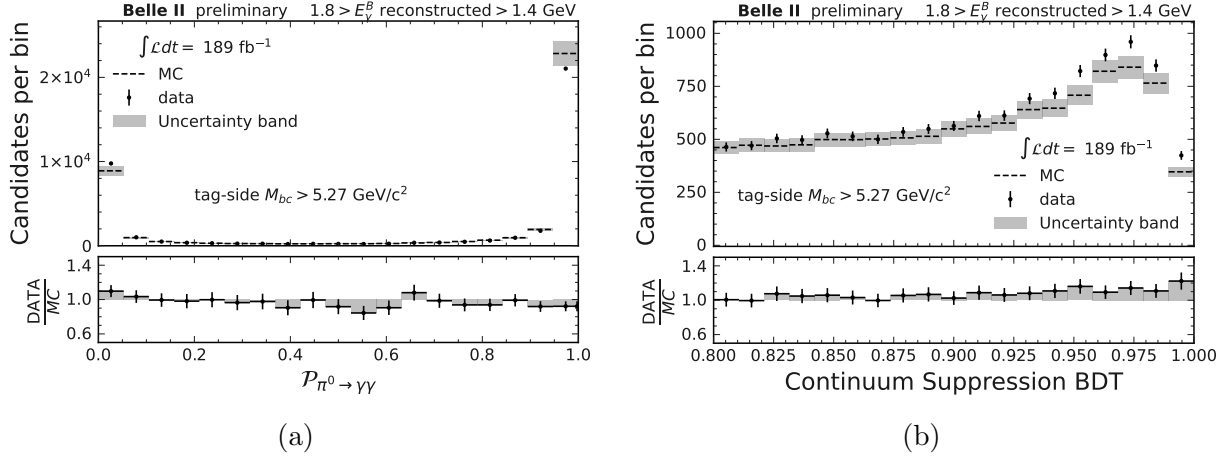


FIG. 4: π^0 rejection veto (Figure 4a) and trained BDT classifier distribution (Figure 4b) for photon energy sideband, compared in simulation and data. Compared to Figure 1b, this plots shows that higher BDT classifier output values for $B\bar{B}$ -like events are described well.

1.4 Selection efficiency and photon resolution

The selection efficiency, corrected to represent data and resolution of E_γ^B are shown in Figure 5.

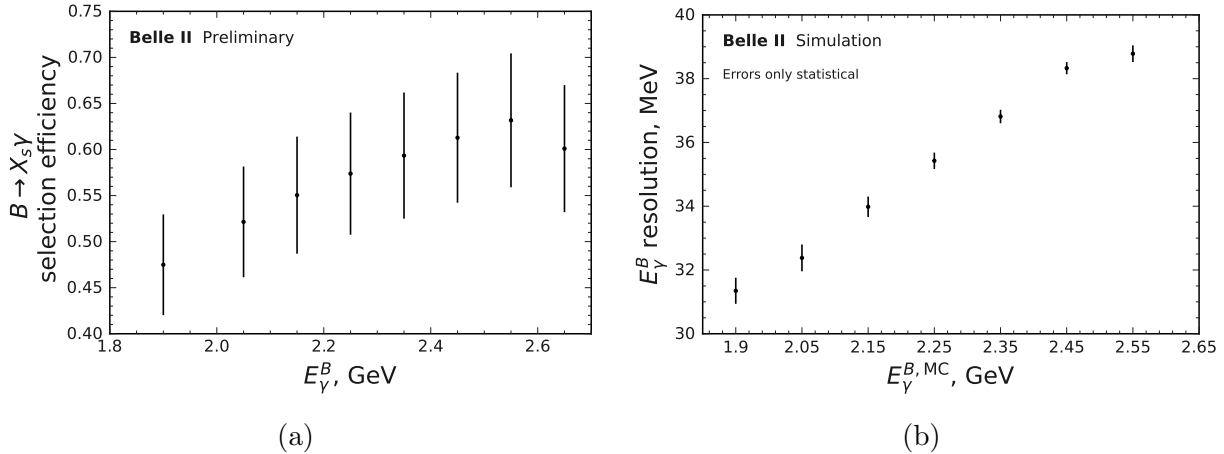


FIG. 5: The selection efficiency (Figure 5a) and photon E_γ^B resolution (Figure 5b) as a function of photon energy. The efficiency uncertainties include correction and additional uncertainties derived in data-driven checks. The resolution only shows simulation-based statistical uncertainties.

1.5 $B \rightarrow X_s\gamma$ spectra

The $B \rightarrow X_s\gamma$ spectra are presented in three forms: no overlay, overlaid with the hybrid-model that we use for unfolding and the hybrid model with the weighted inclusive and $B \rightarrow K^*\gamma$ ingredients explicitly shown. The three versions of the plot are shown in Figure 6.

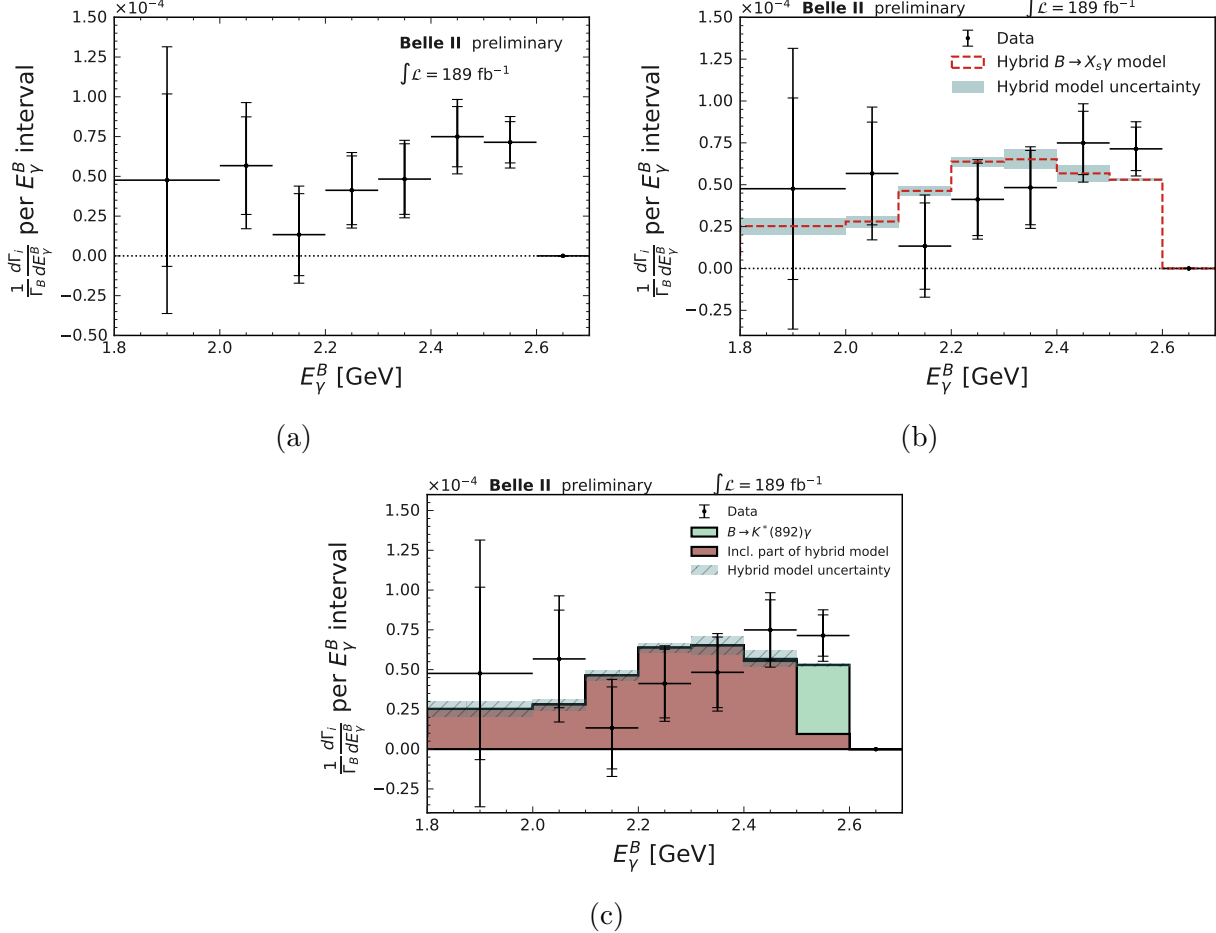


FIG. 6: The extracted number of $B \rightarrow X_s\gamma$ events, as explained in the main conference document. Figure 6a shows the extracted spectrum on data, whereas Figures 6b and 6c also overlay the hybrid-model expectation used in this study. The model uncertainty is based on the inclusive and resonant branching fraction uncertainties as well as the model-shape parameter uncertainties derived from the reference given in the main conference document. The inclusive $B \rightarrow X_s\gamma$ and resonant $B \rightarrow K^*\gamma$ contributions are combined using a hybrid modelling technique which reweights the inclusive model as explained in the main conference note document.

1.6 Fits on all E_γ^B bins

Fits on all E_γ^B bins on data in the control regions are shown in Figure 7. The signal region fits are also given in Figure 8. The latter are equivalent to the plots in the main body. The legend for these figures is provided in Figure 7. It is equivalent to the legend of Figure 8.

1. Fits on the control regions

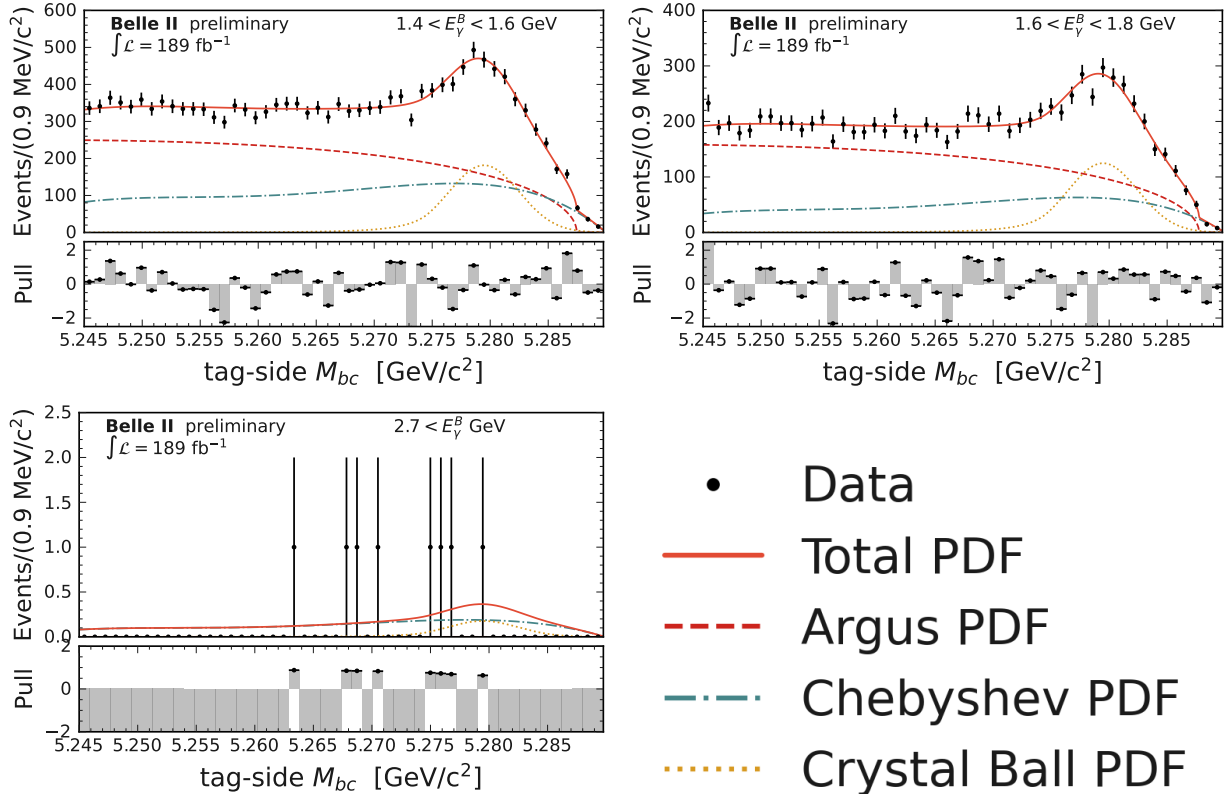


FIG. 7: Fits on all E_γ^B bins within the control regions $1.4 < E_\gamma^B < 1.6$ GeV and $2.7 < E_\gamma^B$ GeV.

2. Fits on the signal regions

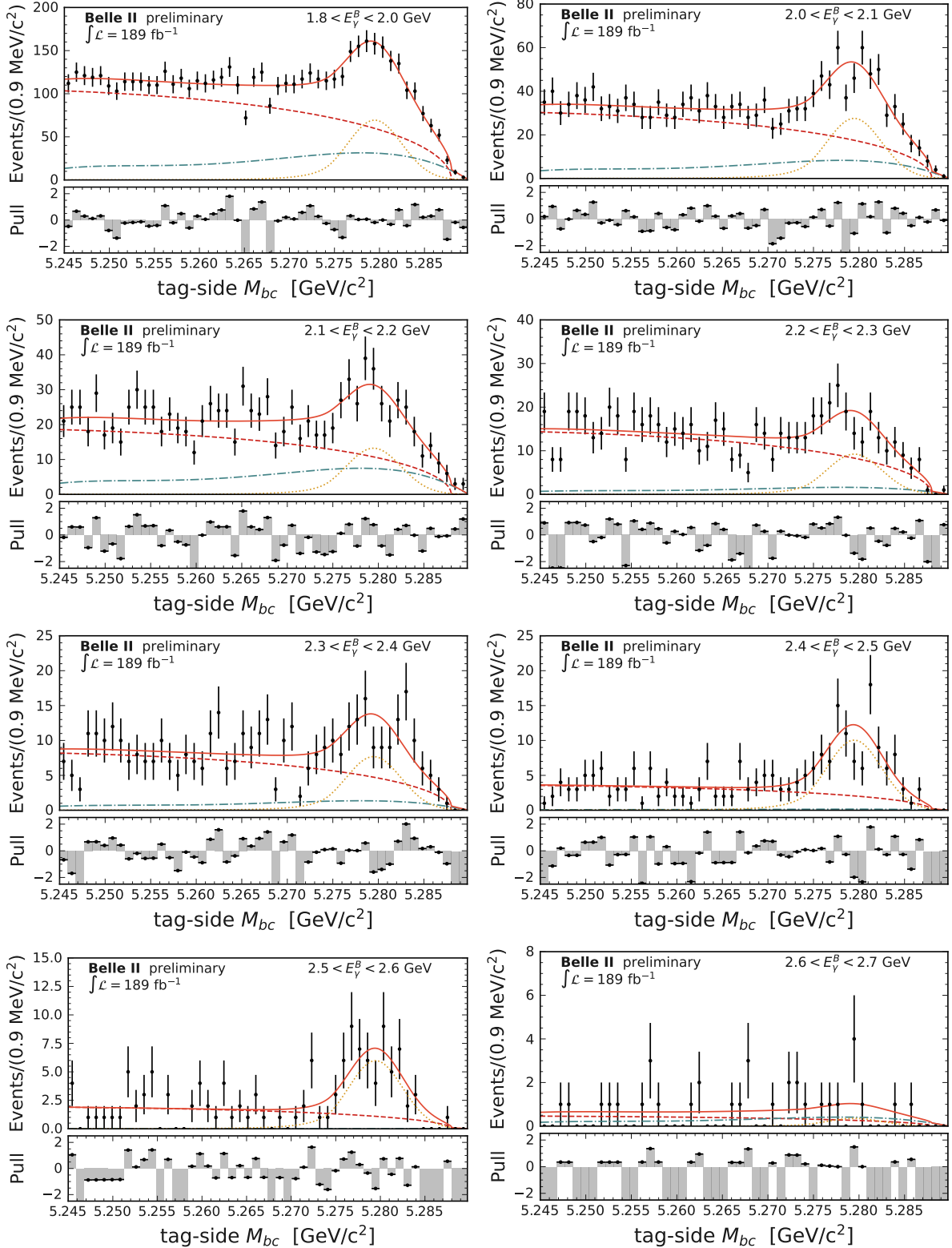


FIG. 8: Fits on all E_γ^B bins within the signal region $1.8 < E_\gamma^B < 2.7 \text{ GeV}$.

1.7 Fitted yields on data

This section contains the figures with the extracted yields in data in linear and logarithmic scale. The figures are given in

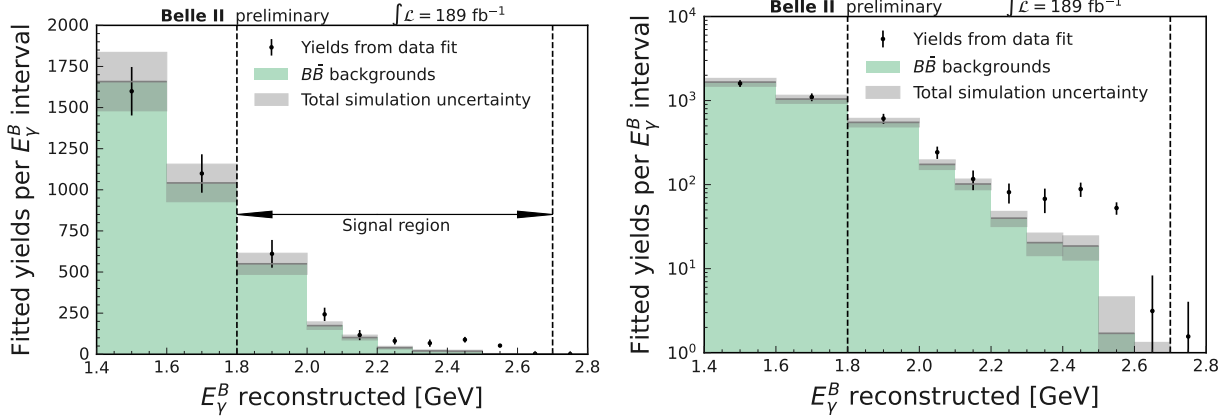


FIG. 9: The peaking- B yields from fits on M_{bc} distributions shown in Figures 7 and 8. The yields are shown in linear and logarithmic scale.

2 Analysis numbers

This section contains numbers of extracted peaking- B yields from data fits; corrected and scaled for luminosity MC peaking- B predictions; efficiency values with uncertainty; and the unfolding factors. All values are given with corresponding uncertainties. Together they form all the numbers required to calculate the branching fraction of $B \rightarrow X_s \gamma$, according to the provided equation in the main text of the note.

E_γ^B [GeV]	Data fit (stat. unc.) (tot. unc.)	Corrected, scaled MC background fit (tot. unc.)	Corrected efficiency ($\times 10^2$) (tot. unc.)	Bin-by-bin unfolding factors (tot. unc.)
1.8 – 2.0	611 (65) (84)	550 (64)	0.211 (0.025)	0.684 (0.130)
2.0 – 2.1	242 (35) (41)	174 (22)	0.232 (0.028)	0.791 (0.091)
2.1 – 2.2	116 (27) (31)	101 (15)	0.245 (0.029)	0.905 (0.048)
2.2 – 2.3	81 (21) (22)	40 (8)	0.255 (0.031)	1.050 (0.029)
2.3 – 2.4	68 (21) (22)	20 (6)	0.263 (0.032)	1.112 (0.093)
2.4 – 2.5	88 (17) (17)	19 (6)	0.272 (0.033)	1.207 (0.141)
2.5 – 2.6	53 (9) (9)	2 (3)	0.281 (0.034)	1.626 (0.057)
2.6 – 2.7	3 (4) (5)	0 (1)	0.267 (0.032)	0.000 (0.000)
